J. Cent. South Univ. (2024) 31: 4082−4097
DOI: https://doi.org/10.1007/s11771-024-5812-3

Springer

Friction surfacing of hypereutectic Al-Si alloy on commercially pure aluminum: Effect of consumable rod heat treatment and heat input

BARARPOUR Seyedeh Marjan[1], JAMSHIDI AVAL Hamed[1]*, JAMAATI Roohollah[1], JAVIDANI Mousa[2]

1. Department of Materials Engineering, Babol Noshirvani University of Technology, Shariati Avenue, Babol 47148-71167, Iran;
2. Department of Applied Science, University of Québec at Chicoutimi, Saguenay QCG7H 2B1, Canada

Abstract: This study investigated the effect of pre-friction surfacing heat treatment of consumable rods and heat input during friction surfacing on the microstructure, mechanical properties, and wear resistance of hypereutectic Al-Si alloy deposited on a commercially pure aluminum substrate. The results show that regardless of the consumable rod's heat treatment conditions, the coating's efficiency has increased with the increase in heat input, so the coating efficiency increases by 20% and 30% in the solid solution-treated rod and the artificially aged rod, respectively. By increasing the heat input, the average grain size in the coating fabricated by solid solution-treated rod and artificially aged rod increased from 0.1 to 0.9 μm and from 0.2 to 1.3 μm, respectively. At constant heat input, the average hardness and wear resistance of the coating created in the solid solution-treated rod are lower than those of the artificially aged rod. By decreasing heat input, the wear loss in the coating fabricated by solid solution-treated rod and artificially aged rod decreased by 10% and 20%, respectively, reaching 0.1 and 0.03 μg/m.

Key words: friction surfacing; hypereutectic Al-Si alloy; heat input; microstructure; wear resistance

Cite this article as: BARARPOUR Seyedeh Marjan, JAMSHIDI AVAL Hamed, JAMAATI Roohollah, JAVIDANI Mousa. Friction surfacing of hypereutectic Al-Si alloy on commercially pure aluminum: Effect of consumable rod heat treatment and heat input [J]. Journal of Central South University, 2024, 31(11): 4082−4097. DOI: https://doi.org/10.1007/s11771-024-5812-3.

1 Introduction

According to the industry's needs, the materials used should be designed to have the longest lifespan and be the most efficient. Increasing the life of materials by improving their surface properties is possible to a large extent, because in engineering applications, the surface of materials is, in the first place, exposed to factors such as corrosion, wear, and shear and tensile forces [1 − 4]. Surface engineering is a tool to simultaneously improve materials' surface and bulk properties so that a piece with a hard surface and a core with high toughness can be prepared [5 − 8]. Different processes have been created to increase the material surface's resistance to corrosion, wear, and failure [8−10]. In addition to increasing the life of the material, these processes also increase its efficiency by changing the properties of the surface layer compared to the substrate. This technology includes coating methods, including physical and chemical vapor phase deposition, laser cladding, thermal spray, and methods that can change the material's surface properties [11−13].

Received date: 2023-10-11; **Accepted date:** 2024-06-10
Corresponding author: JAMSHIDI AVAL Hamed, PhD, Associate Professor; E-mail: h.jamshidi@nit.ac.ir; ORCID: https://orcid.org/0000-0002-5431-0413

Surface engineering in two branches, surface processing and coating, increases the lifespan of materials. In processing methods, modifying the surface leads to improved properties, but in coating methods, they cover a secondary material on the material's surface. Some coating methods, such as nitriding, change the surface properties up to 1 mm, while welding-based methods can create a coating with a thickness of 1−20 mm [14]. The two main coating methods are liquid-state and solid-state [15]. Due to the defects and limitations of the liquid-state techniques due to the high temperature of the process, attention has been drawn towards the solid-state methods. Therefore, these methods can be performed at a temperature lower than the melting temperature and do not contain solidification defects. Also, due to the simultaneous effect of temperature and plastic deformation, dynamic recrystallization takes place, creating a fine-grained structure and leading to an increase in strength [16, 17]. Roll bonding, friction surfacing, and explosive cladding are among the methods of solid-state coating [18].

The friction surfacing (FS) process is a solid-state coating method derived from the friction welding method and was proposed for the first time in 1941 by KLAPSTOCK et al [19]. This method can join similar and dissimilar materials together and is an ideal method for metals sensitive to temperature, such as aluminum. Similar to other friction stir-based processes [20], the heat source in the FS process is plastic deformation and friction during the process, and it does not need an external source; it is economical in terms of energy. In this process, the consumable rod is subjected to a vertical force at a certain speed, and with the rotational movement, it causes friction and increases the temperature, and a viscoplastic area is created at the rod's tip. By moving the consumable rod at a specific traverse speed, the viscoplastic area is deposited on the sample's surface; it forms a coating layer with a metallurgical-mechanical bond on the surface of the substrate [13, 21, 22].

Considering the properties of pure aluminum, including ductility and high thermal conductivity, this metal is considered a suitable option for use in various industries. However, the lack of alloy elements and low mechanical properties limit its use. According to the studies done on pure aluminum coating with the help of the FS process, various studies have been done by different researchers. These studies include coating aluminum alloy [23 − 26] or aluminum composite [27 − 29]. Aluminum-silicon alloys have a high ability to improve the surface properties of pure aluminum. Aluminum-silicon alloys are widely used in the transportation industry due to their low coefficient of thermal expansion, high hardness and wear resistance, high-temperature strength, and good castability [30, 31]. Silicon is the main alloying element of these alloys, which has caused high wear resistance in these alloys due to their high hardness [32−34]. Considering that alloys with good wear resistance can be used to replace or repair industrial parts, aluminum-silicon hypereutectic alloys can be used as a suitable option to improve mechanical and tribological properties as a coating material. In previous studies by BARARPOUR et al [35−37] and SCHÜTTE et al [38], friction surfacing of Al-Si alloy coating was studied. Studies have shown that, despite the effect of process parameters on the microstructure and properties of the coating, the heat treatment conditions of the consumable rod have a significant impact on the properties of the coating [39]. A critical point identified in the review of various sources is that the simultaneous effect of heat input and the consumed rod's initial conditions on the coating's properties and microstructure has not been studied. In this research, taking into account the two conditions of solid solution-treated and artificially aged consumable rods, the effect of two different heat inputs on the microstructure, mechanical properties, and wear resistance of the Al-Si alloy friction surfaced on the AA1050 aluminum substrate has been studied.

2 Experimental procedures

2.1 Friction surfacing

In this research, friction surfacing was performed at two different heat inputs, considering rotational speed, axial feeding rate, and traverse speed of 1000 r/min, 125 mm/min, and 75 mm/min, respectively for the maximum heat input state; and

rotational speed, axial feeding rate, and traverse speed of 600 r/min, 95 mm/min, and 115 mm/min, respectively for the minimum heat input state. The selection of the process parameters has been made by considering the rotational speed in the range of 600−1000 r/min, the axial feeding rate in the range of 95−125 mm/min, the traverse speed in the range of 75−115 mm/min, and measuring the temperature at the interface between the coating and the substrate. The coating parameters that led to the minimum and maximum temperature were selected as the parameters that produced the maximum and minimum heat input. As shown in Figure 1, a customized milling machine was used for friction surfacing.

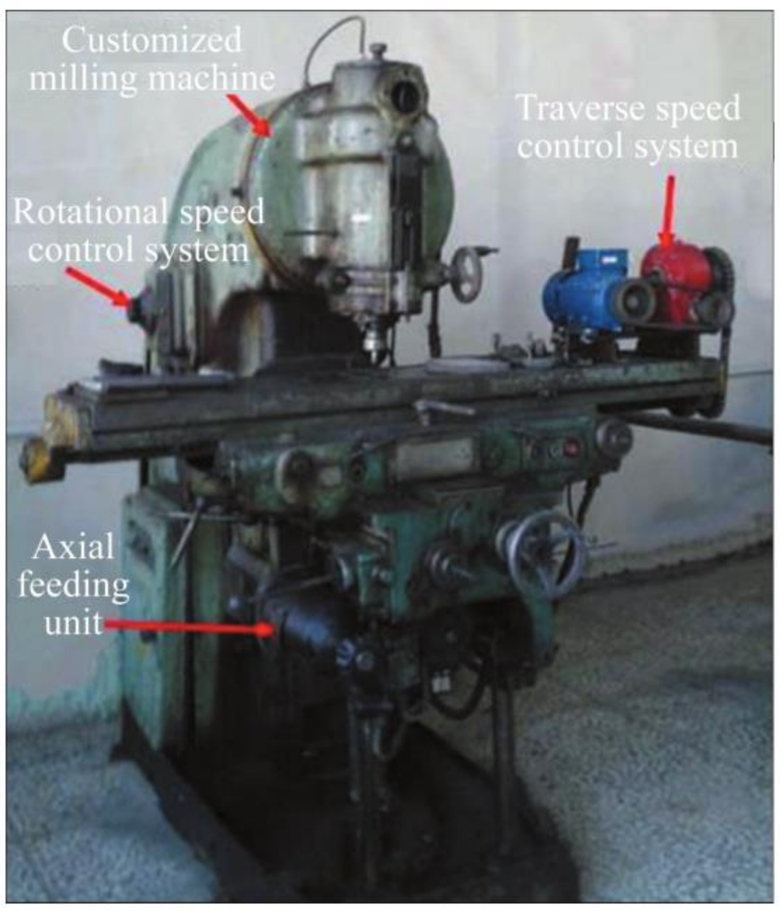

Figure 1 Experimental setup used in this study

2.2 Materials

The coating was done using an Al-Si hypereutectic alloy rod with the composition of 16.18% Si, 4.1% Cu, 0.48% Mg, 0.11% Fe, 0.09% Zn, 0.08% Ti, 0.02% Mn, and Al balance (wt%). The consumable rods were prepared from Al-Si cast alloy and machined as rods with a diameter of 20 mm and a length of 200 mm. The coating was done on an AA1050 aluminum substrate with a chemical composition of 0.07% Si, 0.28% Fe, 0.05% Cu, 0.02% Mn, 0.01% Mg, and Al balance (wt%) with a thickness of 4 mm and area of 100 mm×100 mm. The solid solution treatment involved heating the consumable rod at 500 ℃ for 8 h and then rapidly quenching in water at 25 ℃. In the case of artificial aging, the consumable rod was heated at 145 ℃ for 15 h after the solid solution treatment.

2.3 Coating characterization

The coated samples with different consumable rods and different heat inputs were named according to Table 1. In order to study the microstructure of the coatings, the coated samples were cut perpendicular to the coating direction. The cross-section of the metallographic samples was prepared by polishing with SiC sandpaper and polishing with alumina suspension. The Keller etchant solution with the composition of 3 mL nitric acid (HNO_3), 6 mL hydrofluoric acid (HF), 6 mL hydrochloric acid (HCl), and 150 mL H_2O was used to reveal the microstructure of the coating. The microstructure was investigated by optical and scanning electron microscopes.

To evaluate the strength of the coatings, the shear punch test (SPT) was performed at room temperature using a SANTAM STM-250 universal testing machine with a punch speed of 0.1 mm/min, following the method outlined in Ref. [40]. The coatings' wear resistance was assessed using a pin-on-disc tribometer wear test. A cylindrical pin with a height and diameter of 7 mm and 3 mm was worn on a disc made of ASIS/SAE 42100 steel with a hardness of 60 HRC at a sliding speed of 50 mm/s. The load was set at 10, 30 and 50 N, and the distance was set at 5000 m, respectively. The push-

Table 1 Friction surfaced processed samples labeling

Sample label	Rotational speed/ ($r \cdot min^{-1}$)	Traverse speed/ ($mm \cdot min^{-1}$)	Axial feeding rate/ ($mm \cdot min^{-1}$)	Consumable rod heat treatment
Sample LH-SS	600	115	95	Solid solution, 402 ℃
Sample HH-SS	1000	75	125	Solid solution, 451 ℃
Sample LH-T6	600	115	95	Artificially aging, 398 ℃
Sample HH-T6	1000	75	125	Artificially aging, 422 ℃

off test (POT) was used to investigate the joint's strength at the interface of coatings. The POT was performed according to the method described by NIXON et al [41]. The micro-Vickers hardness of the samples was measured using a KOOPA-MH4 microhardness tester, applying a load of 0.98 N and a dwell time of 10 s along the central line of the coating perpendicular to the coating direction.

3 Results and discussion

3.1 Coating morphology and efficiency

In order to investigate the effect of heat treatment on the consumable rod and heat input, the cross-section of different samples is shown in Figure 2. The geometric dimensions of the coating and the efficiency of the coatings are reported in Figure 3. In order to calculate the coating efficiency, calculations were performed using the method mentioned in Ref. [42] as follows:

$$\eta_{\text{coating}} = \eta_{\text{deposition}} \cdot \eta_{\text{joining}} \tag{1}$$

$$\eta_{\text{deposition}} = \frac{Av_x}{\pi r^2 v_z} \tag{2}$$

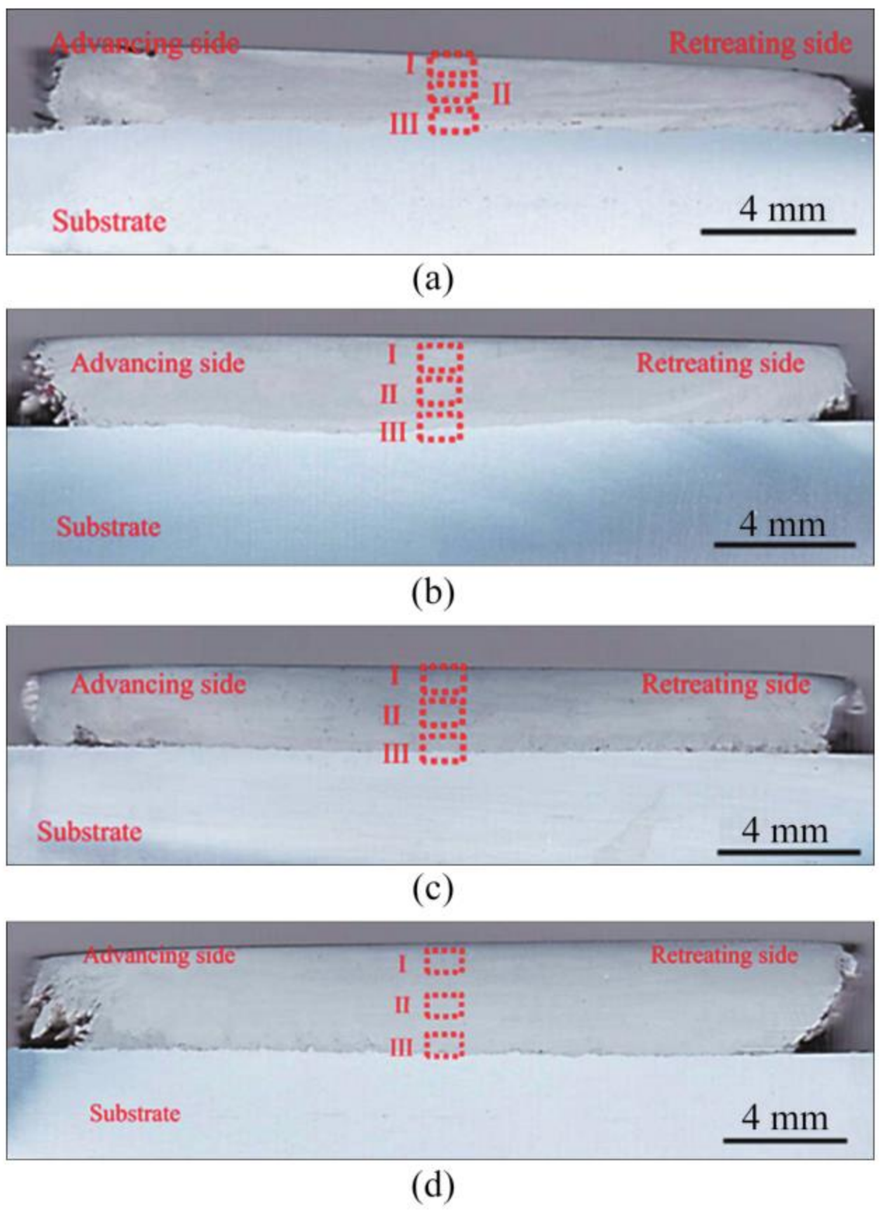

Figure 2 Cross section of different coatings: (a) Sample LH-SS; (b) Sample HH-SS; (c) Sample LH-T6; (d) Sample HH-T6

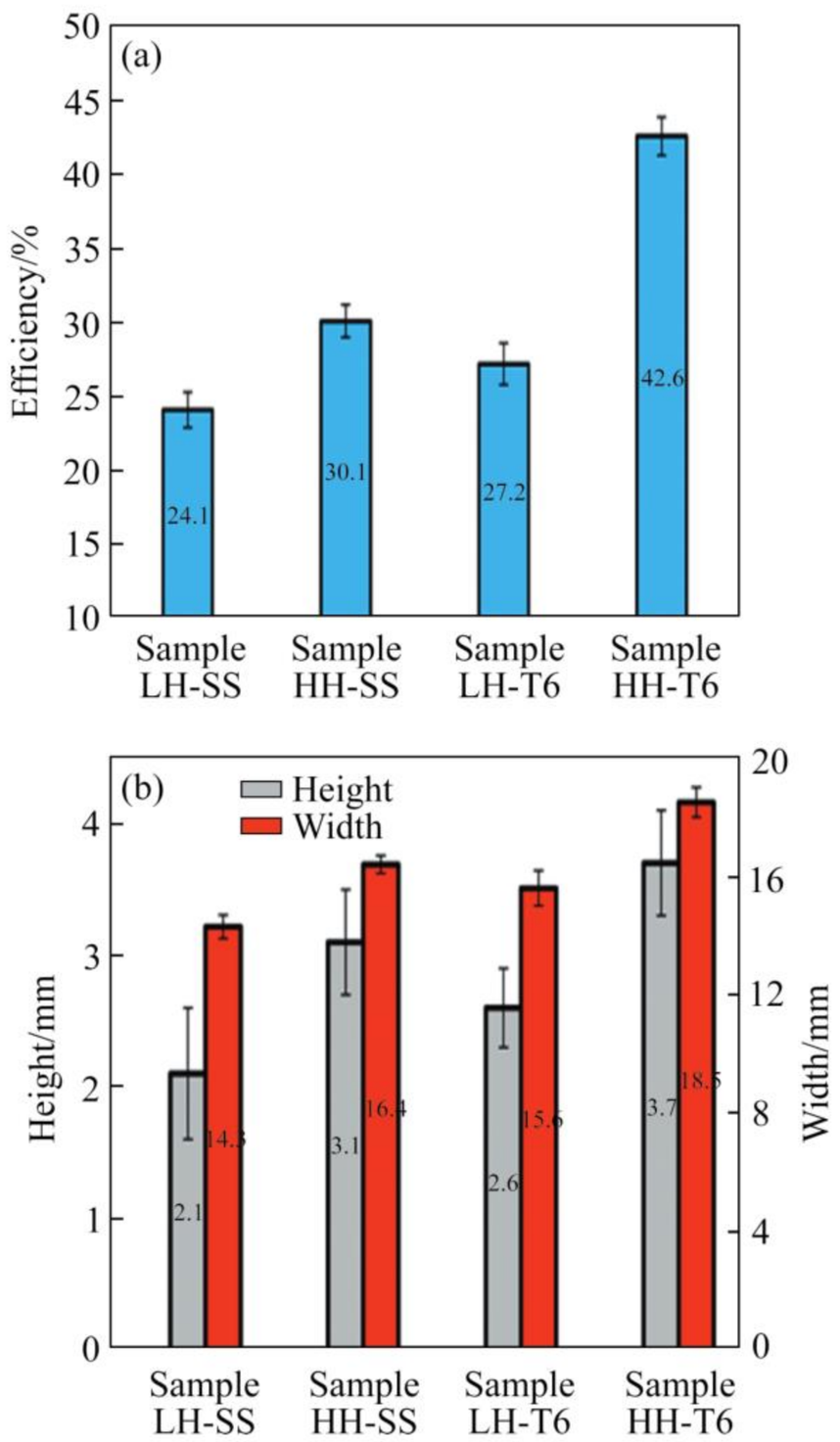

Figure 3 Coating efficiency (a) and dimensions (b) of coating

$$\eta_{\text{joining}} = \frac{W_{\text{b}}}{W_{\text{a}}} \tag{3}$$

where A, v_x, v_z, r, W_{b} and W_{a} are the area of the coating cross-section, traverse speed, axial feeding rate, radius of the consumable rod, bonded coating widths, and maximum coating widths, respectively. As can be seen, regardless of the heat treatment conditions of the consumable rod, the efficiency of the coating has increased with the increase in heat input, so that the coating efficiency increases by 25% and 57% in the solid solution-treated rod and the aged rod with the rise in heat input, respectively. With the increase in heat input, the flow of the material at the tip of the consumable rod is done more easily, and as a result, the amount of material deposited on the surface of the substrate increases. The remarkable result is that in the solid solution-treated rod, with the rise in heat input, the increase in coating efficiency is far less than that of the aged rod.

The temperature of the rod tip used in samples LH-SS, HH-SS, LH-T6, and HH-T6 is 402, 451, 398, and 422 ℃, respectively. The consumable rod's temperature is higher than the aging temperature of the Al-Si hypereutectic alloy [43]. Therefore, it can be expected that with the increase in heat input, there is a possibility of aging at the tip of the consumable rod, which will increase the flow ability of the material at the tip of the consumable rod following the continuation of the process and the increase in the possibility of the occurrence of the over-aging phenomenon. Of course, it should be noted that, compared to the artificially aged rod, a part of the heat input is used for aging in the solid solution-treated rod. Therefore, it can be expected that the volume of the deformed material in the artificially aged rod is much higher than that of the solid solution-treated rod; as a result, a higher flow stress is created in the artificially aged rod.

3.2 Microstructure of coating

Figures 4 and 5 show the microstructure of different areas of the coatings, as shown in Figure 2. As can be seen, in comparison with the microstructure of the consumable rod shown in Figure 6, fine and equiaxed grains with a uniform distribution of silicon particles are observed in all coatings. The formation of a uniform distribution of fine silicon particles is compared to the microstructure of the initial rod which contains eutectic silicon with a high aspect ratio as well as massive copper-rich particles, indicating that under the influence of heat and severe plastic deformation during the process, silicon particles with a large

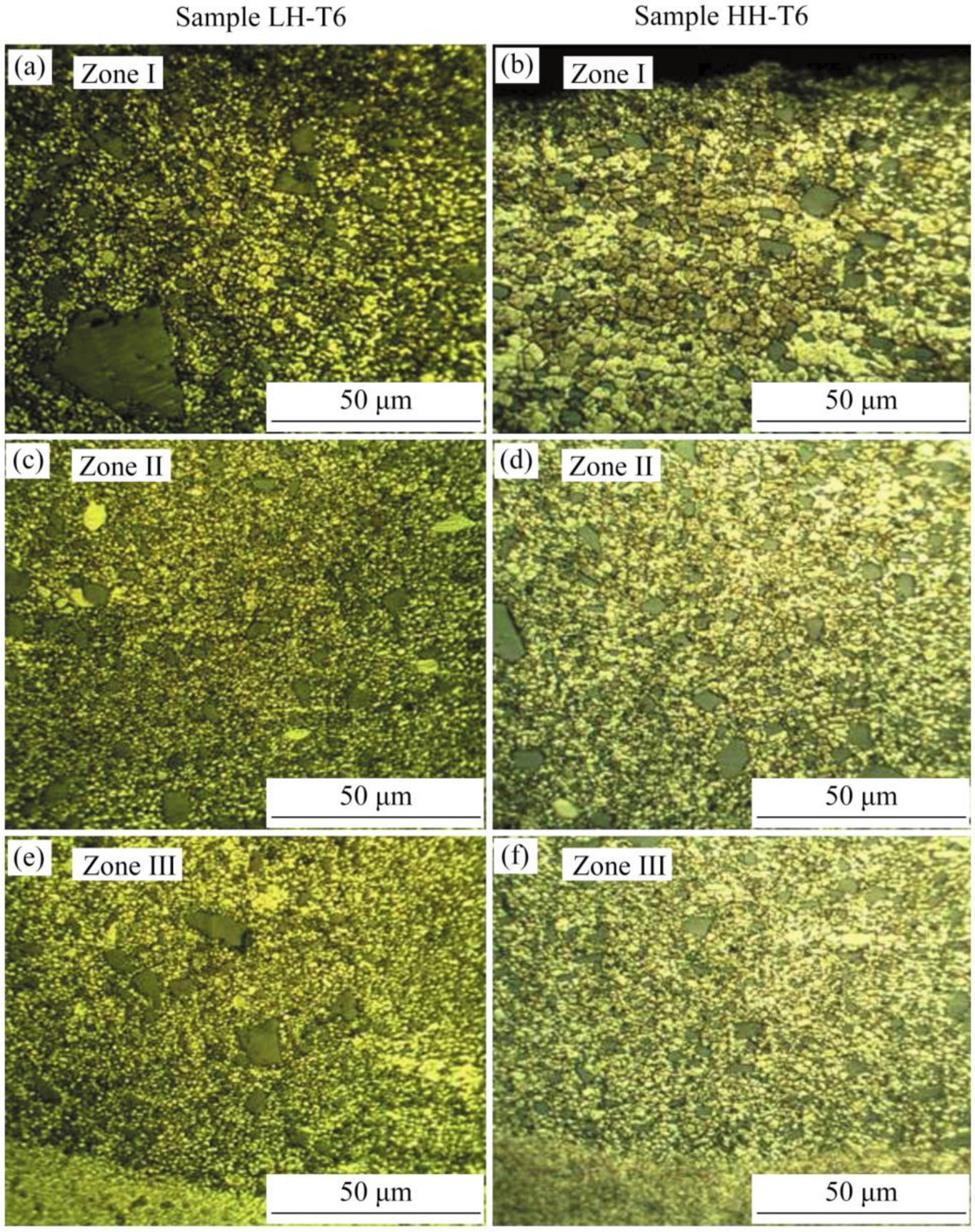

Figure 4 Optical microscopy image of various zones of the samples coated using artificially aged consumable rod (various zones are shown in Figure 2)

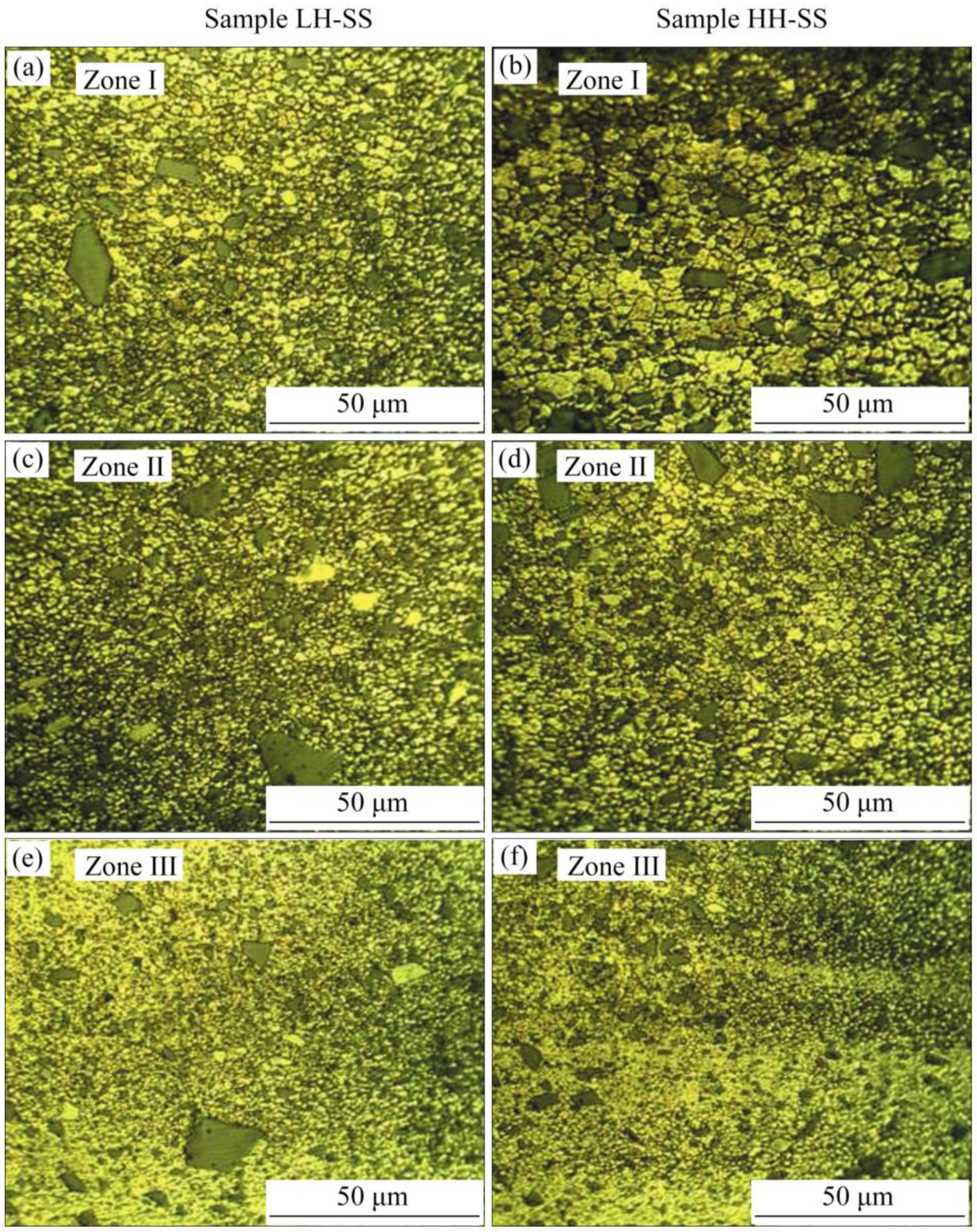

Figure 5 Optical microscopy image of the various zones of the samples coated using solid solution treated consumable rod (various zones are shown in Figure 2)

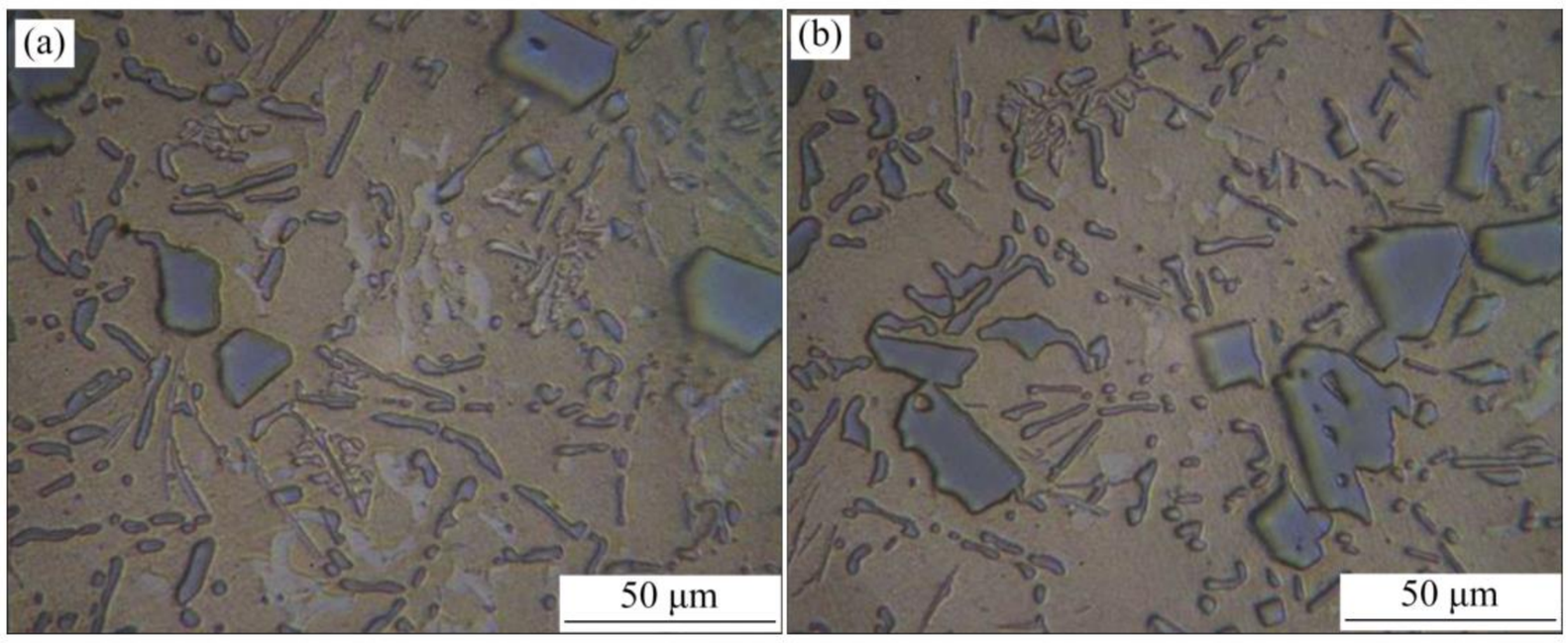

Figure 6 Optical microscopy images: (a) Solid solution treated consumable rod; (b) Artificially aged consumable rod

aspect ratio are broken and transformed into fine particles in the microstructure. The formation of fine and equiaxed grains indicates the occurrence of dynamic recrystallization [44]. According to the coating geometry and the process parameters, and considering the following relationship, the plastic strain rate in different samples is reported in Table 2. According to Refs. [45, 46], temperature

and plastic strain rate are two determining factors in the formation of recrystallized microstructure. With increasing temperature or decreasing plastic strain rate, the recrystallized grain size increases. As can be concluded from the results of grain size and strain rate values presented in Table 2, depending on the heat treatment type of consumable rod, the grain size in the coating increases with increasing temperature and increasing plastic strain rate. According to line intercept method, the average grain size of samples LH-SS, HH-SS, LH-T6, and HH-T6 is (10±1), (12±1), (11±1) and (13±2) μm, respectively. According to [46], while temperature and strain rate have opposing effects on grain size, the increase in grain size with higher heat input indicates that the influence of temperature outweighs the impact of strain rate, resulting in an overall increase in grain size. Since the increases in temperature and strain rate have an opposite effect on grain size, the increase in grain size with the increase in heat input shows that the influence of temperature is dominant over the impact of strain rate, and an increase in grain size occurs. Of course, it should be noted that the higher temperature in the coating created with the solid solution-treated rod has led to grain growth due to the dominance of the temperature effect. The noteworthy point is that from the upper areas of the coating to the interface between the coating and the substrate, the grain size of the coating decreases. At the upper levels of the coating, it seems that despite the higher plastic strain rate than other areas of the coating [47], grain growth occurs due to higher temperatures in this zone, leading to coarser grain size in this area of the coating. In the area near the interface, due to the heat sink caused by the substrate, heat transfer occurs faster to the surrounding environment, which causes grain growth in this area to be prevented, and as a result, fine grains form in the interface area.

Table 2 Average grain size and predicted plastic strain rate of different coatings

Sample label	Grain size/μm	Plastic strain rate/s^{-1}
Sample LH-SS	3.2±0.9	21
Sample HH-SS	6.1±0.7	29
Sample LH-T6	2.2±0.8	24
Sample HH-T6	4.2±0.6	35

Figure 7 shows the distribution of silicon particles in different coatings. As can be seen, regardless of the heat treatment condition of a consumable rod, the size of the silicon particles decreases, and a more uniform distribution of particles is created in the coating. Meanwhile, in the coating created with a solid solution-treated rod, due to the formation of a higher temperature during the coating, the aluminum surface will become softer, and a smaller shear stress will be applied to the silicon particles. In this situation, it is possible to break silicon particles and distribute them in a matrix.

In this way, it can be expected that a non-uniform distribution of silicon particles with larger silicon particles will form in the coating created by the solid solution-treated rod. The SEM images of the central area of the coating in different samples are shown in Figures 8 and 9. Also, the SEM images of consumable rods are shown in Figure 10. The

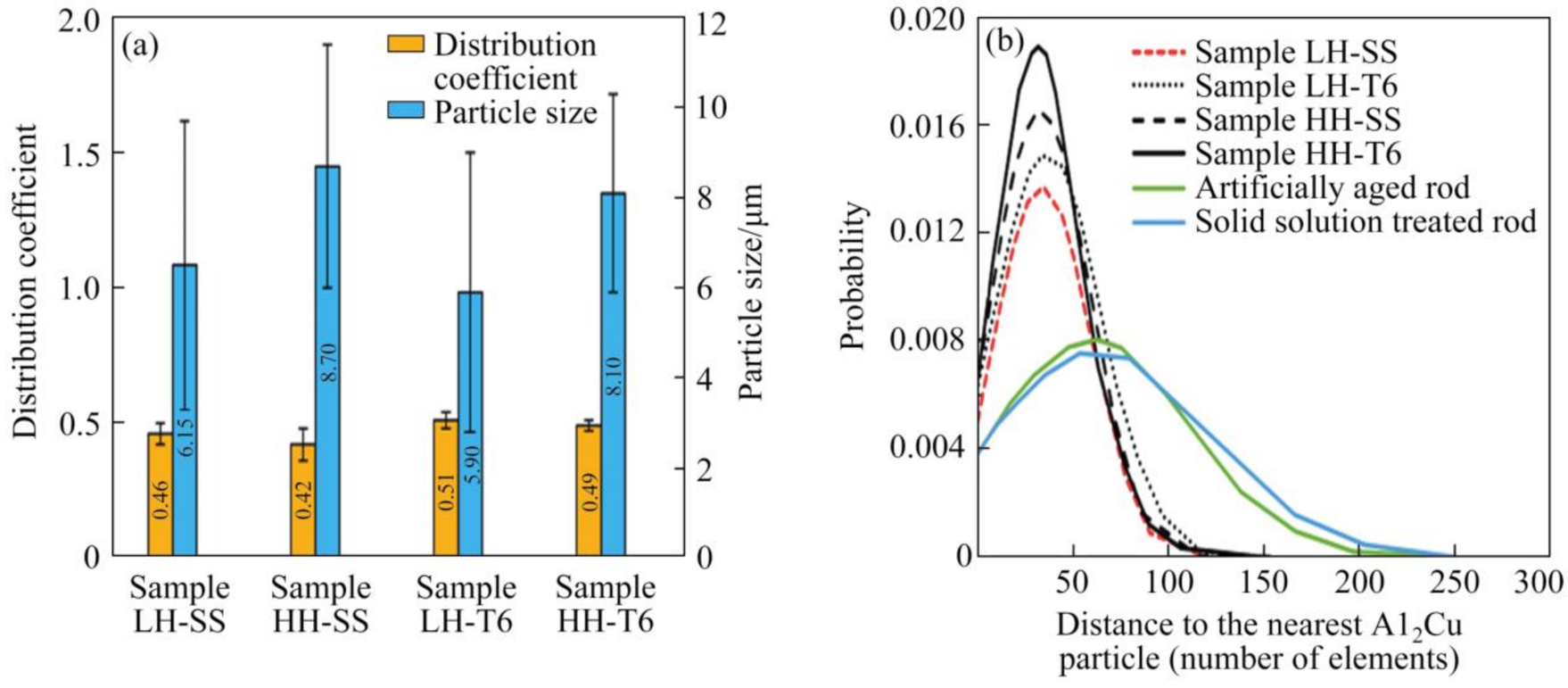

Figure 7 (a) Distribution coefficient and size of Si particles in different samples; (b) Probability density function of distance to the nearest Si particle for different samples

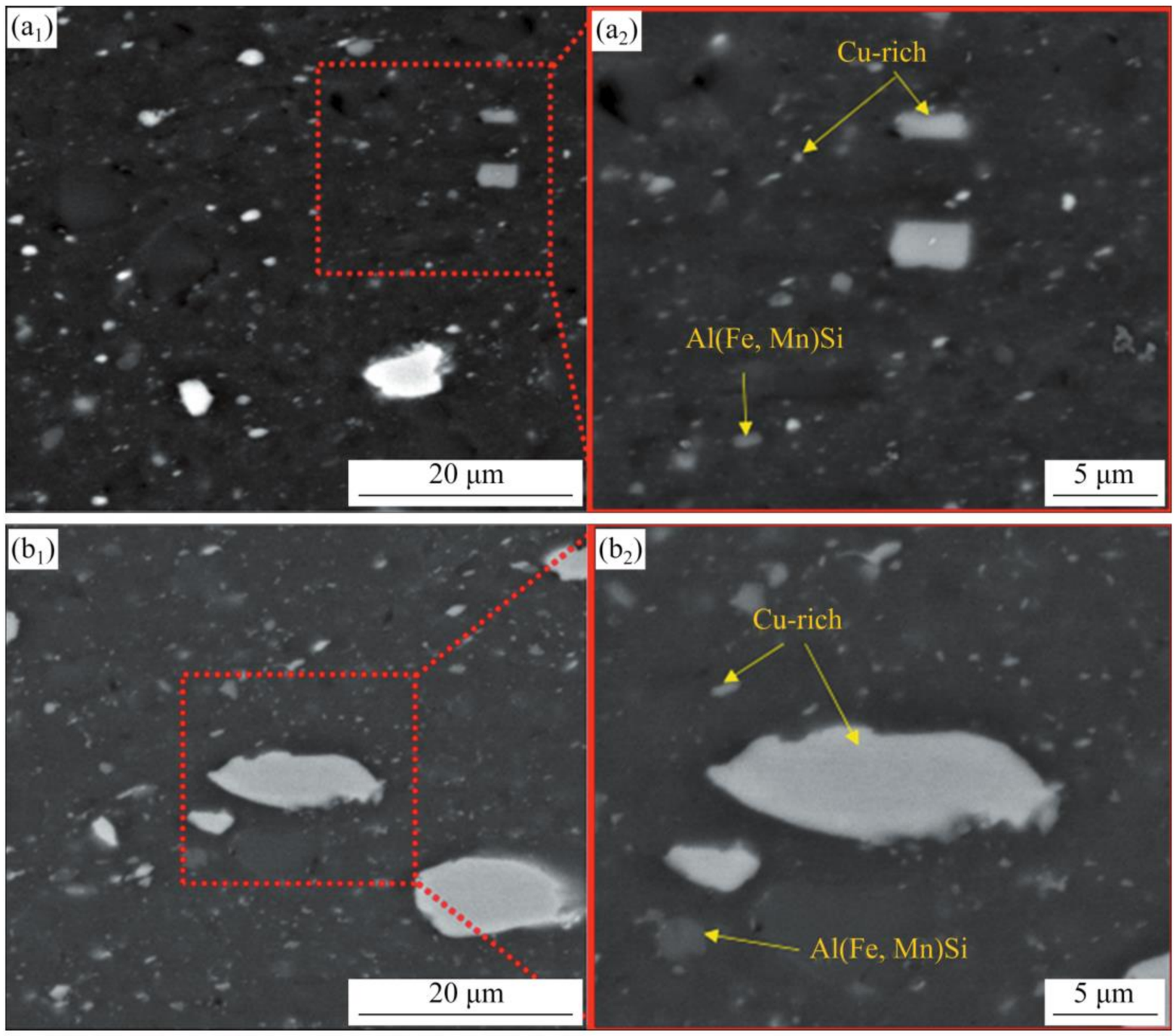

Figure 8 SEM images of center zone: (a) Sample LH-SS; (b) Sample HH-SS

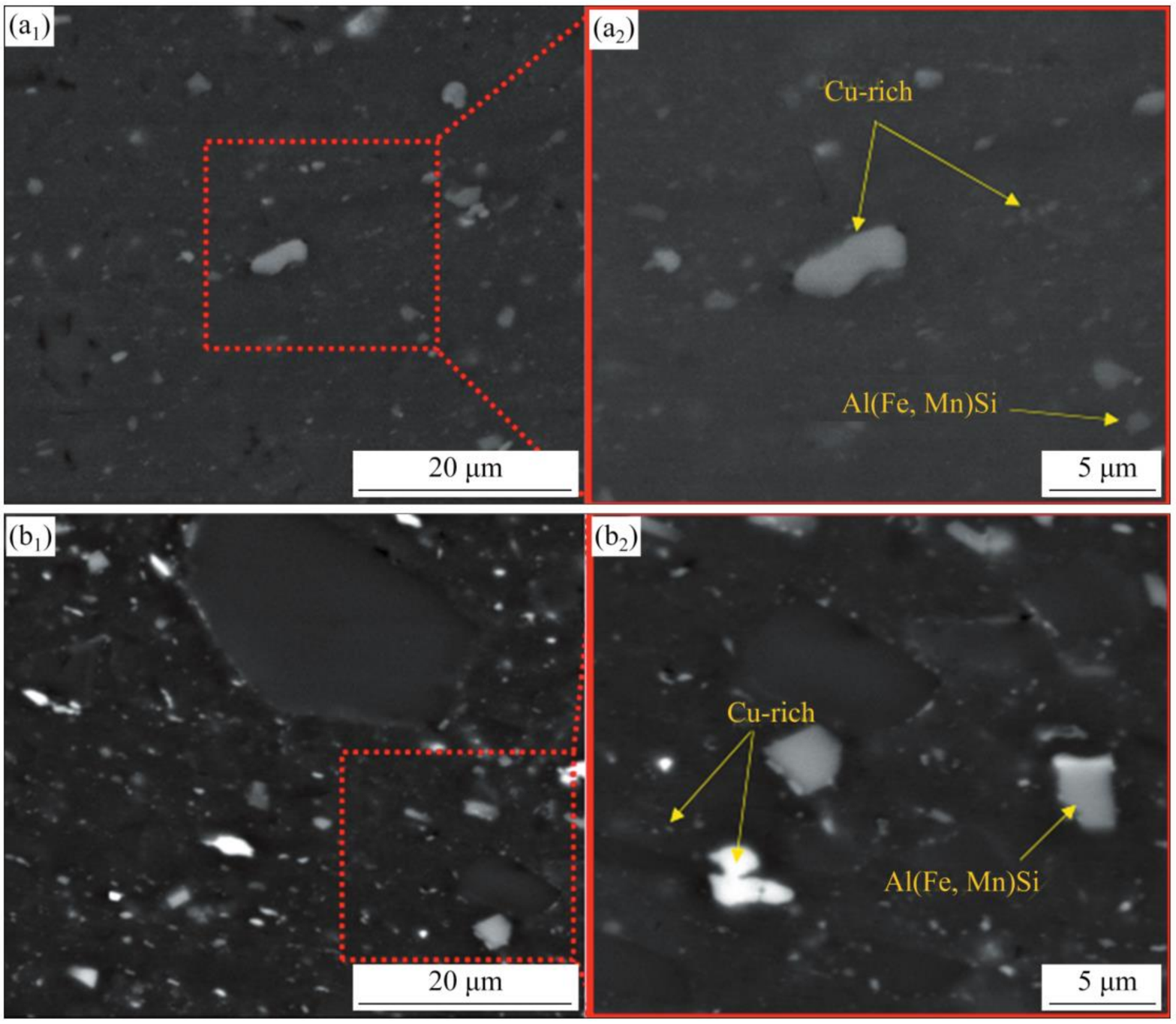

Figure 9 SEM images of center zone: (a) Sample LH-T6; (b) Sample HH-T6

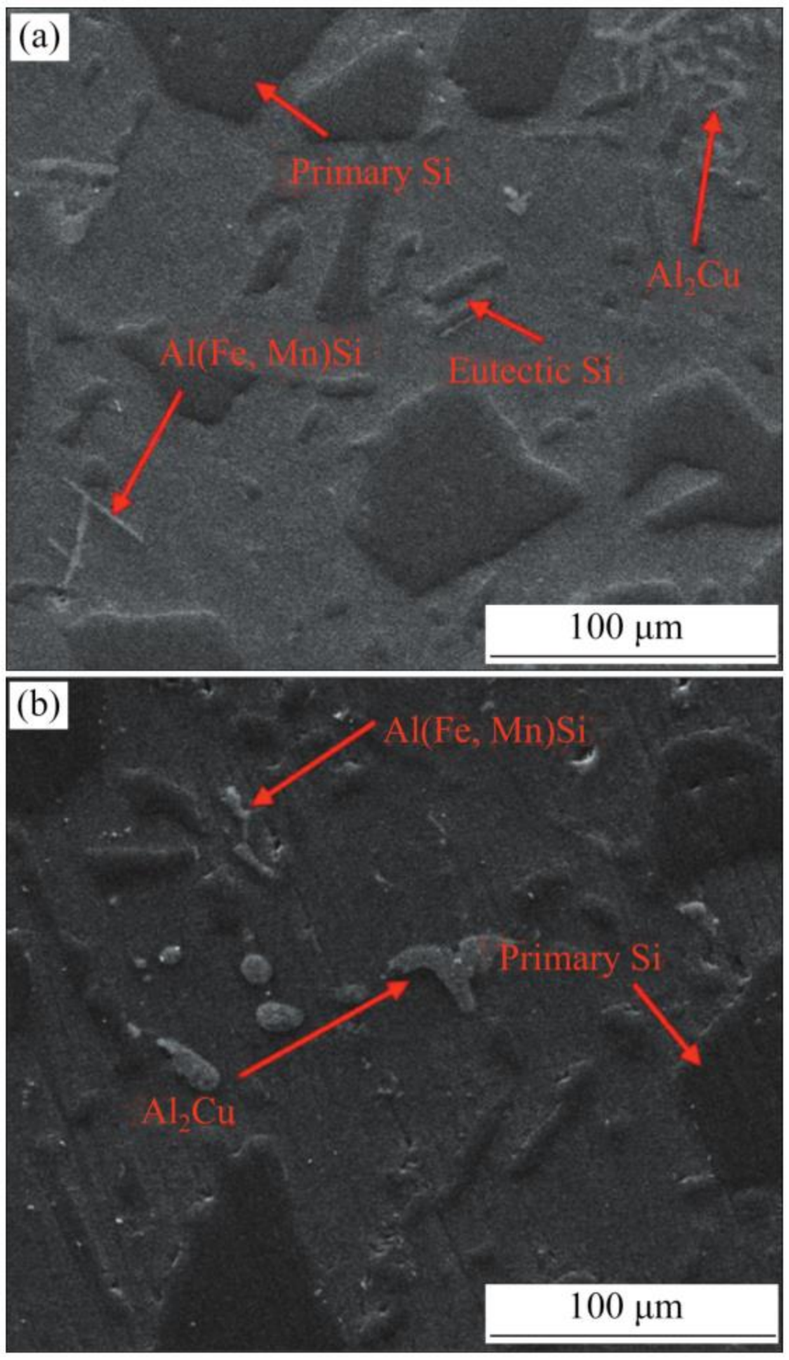

Figure 10 SEM images of microstructure: (a) Solid solution treated consumable rod; (b) Artificially aged consumable rod

coatings contain silicon particles, copper-rich particles, and iron-rich particles. An important point that can be seen in the comparison of the images of the coating and the consumable rod is the significant reduction in the size of copper and iron-rich particles in the coatings. Since iron-rich particles cannot dissolve during coating, these coarse particles in the consumable rod break during the FS process due to the strain applied during the process, and as a result, fine iron-rich particles in the microstructure are formed.

Meanwhile, according to image analysis, the size of the iron-rich particles in the coating created in the solid solution-treated rod is more significant than that of the artificially aged rod (Figure 11). The average sizes of iron-rich particles in samples LH-SS, HH-SS, LH-T6, and HH-T6 are (3.2±1.1), (3.8±1.2), (2.4±1.4) and (3.4±1.3) μm, respectively. It can be concluded that high temperature during friction surfacing causes lower flow stress to be applied to the particles, and as a result, a smaller size reduction can be seen in these particles. The

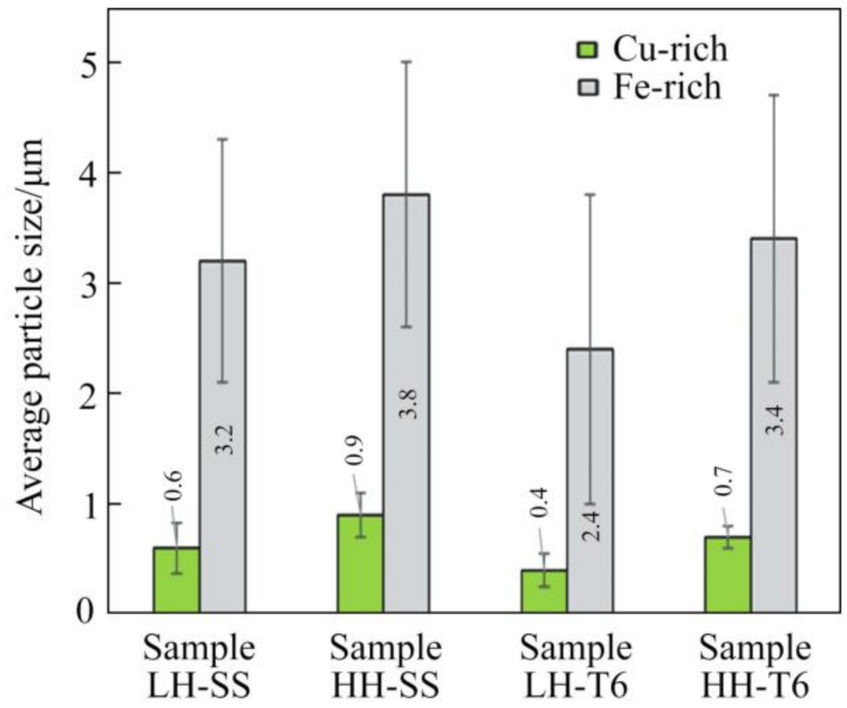

Figure 11 Average particle size of Cu-rich and Fe-rich particles

copper-rich particles can dissolve in the aluminum matrix under the influence of temperature and plastic strain rate during the process and re-precipitation in the coating during cooling. Although re-precipitation conditions do not occur for all copper-rich particles, it can be expected that the conditions for re-precipitation are not easily provided by reducing the temperature during coating and increasing the cooling rate. In this situation, it can be expected that the precipitates formed due to re-precipitation in the coating created with the solid solution rod will be greater.

On the other hand, the copper-rich particles are not easily broken due to the lower stress applied by the matrix to the copper-rich precipitates in the coating created with the solid solution-treated rod. In general, it can be said that the smaller copper-rich particles in the coating created with the artificially aged rod mean that the breaking of copper-rich particles during the process causes the copper particles to become smaller, and the effect of this mechanism on the formation of copper-rich particles in the coating is much higher. The average size of copper-rich particles in samples LH-SS, HH-SS, LH-T6, and HH-T6 is (0.6±0.2), (0.9±0.2), (0.4±0.1) and (0.7±0.2) μm, respectively.

3.3 Hardness and bond strength of coating

The changes in hardness and average hardness of the coating in different samples are shown in Figure 12. In all coatings, regardless of the heat treatment conditions of the rod and heat input, the hardness value decreases from the top of the coating

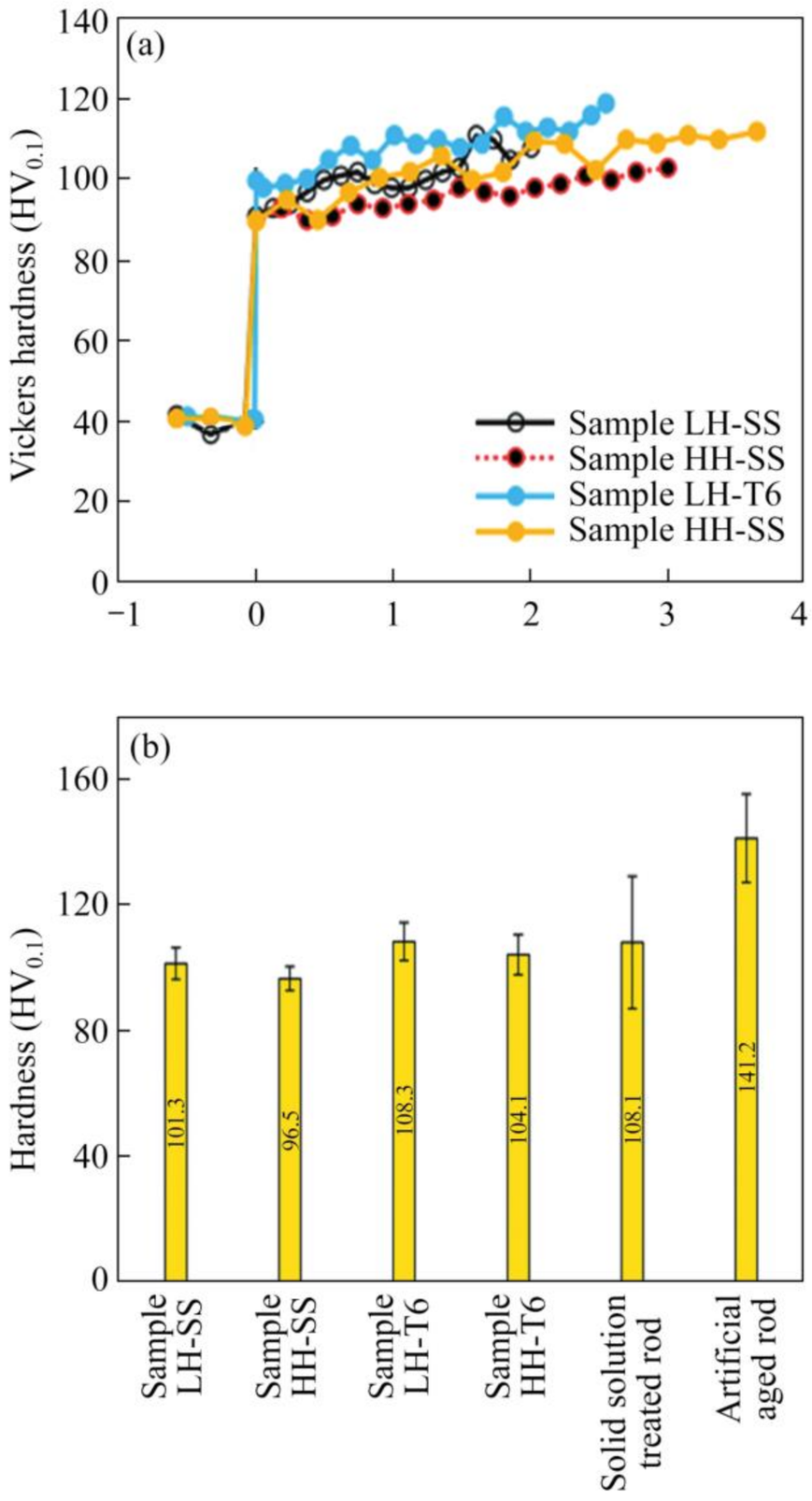

Figure 12 (a) Micro-hardness profile along centerline of coating; (b) Average hardness of different samples

towards the interface of the coating. According to the obtained results, it can be said that the smaller grain size and smaller silicon particles in the upper areas of the coating can be the main reason for the greater hardness in the upper areas of the coating. According to the hardness values, it can be seen that the average hardness of the coating decreases with the increase in heat input in both the coating created with the solid solution-treated and the artificially aged consumable rod. The average hardness of samples LH-SS, HH-SS, LH-T6, and HH-T6 is $HV_{0.1}$ (101.3±1.2), $HV_{0.1}$ (96.5±2.1), $HV_{0.1}$ (108.3±1.3) and $HV_{0.1}$ (104.1±2.2), respectively. The formation of larger grains, as well as coarser copper-rich particles and larger silicon particles, can be the main reason for the decrease in hardness of the coating with an increase in heat input.

Meanwhile, at a similar heat input, the average hardness of the coating created with the solid solution-treated rod is lower than that created with the artificially aged rod. The presence of finer grains, smaller copper-rich particles, and smaller silicon particles in the coating created with the artificially aged consumable rod is the main reason for the higher hardness in the coating created with the artificially aged rod. The shear strength results of different coatings are shown in Figure 13. The trend of shear strength changes is similar to the changes in coating hardness, so the coating created with the artificially aged consumable rod leads to more shear strength in the coating, and the shear strength of the coating increases with the decrease in heat input. Meanwhile, according to the results of the bond strength of the coating shown in Figure 14, it can be seen that with the increase in heat input due to the expansion of the coating on a wider

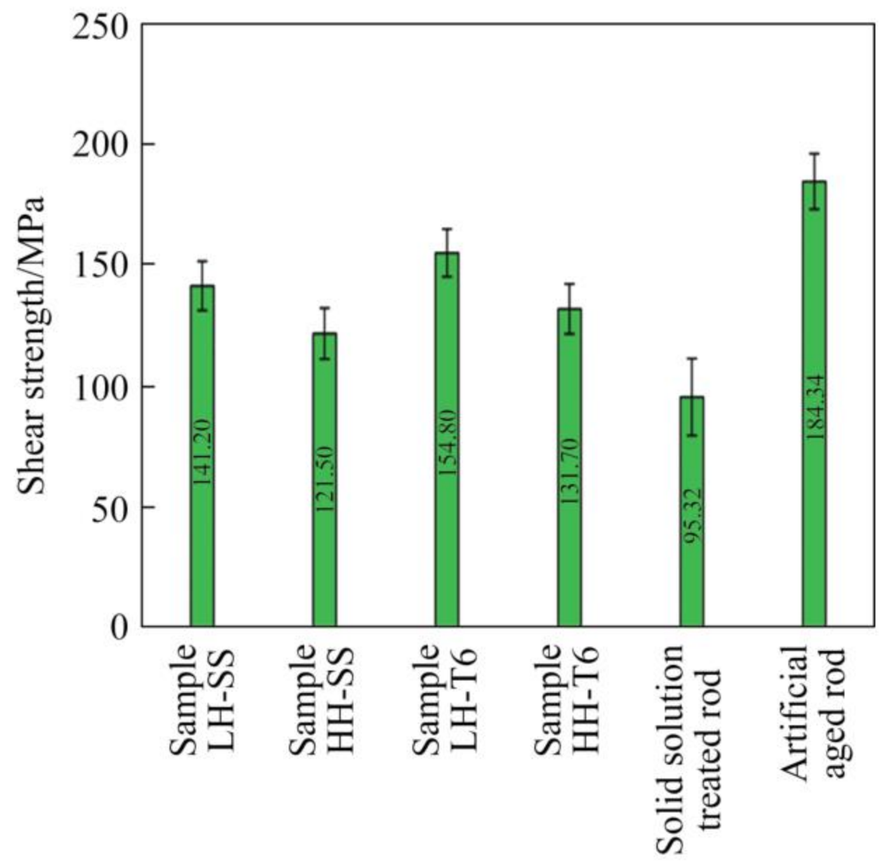

Figure 13 Shear strength of different samples

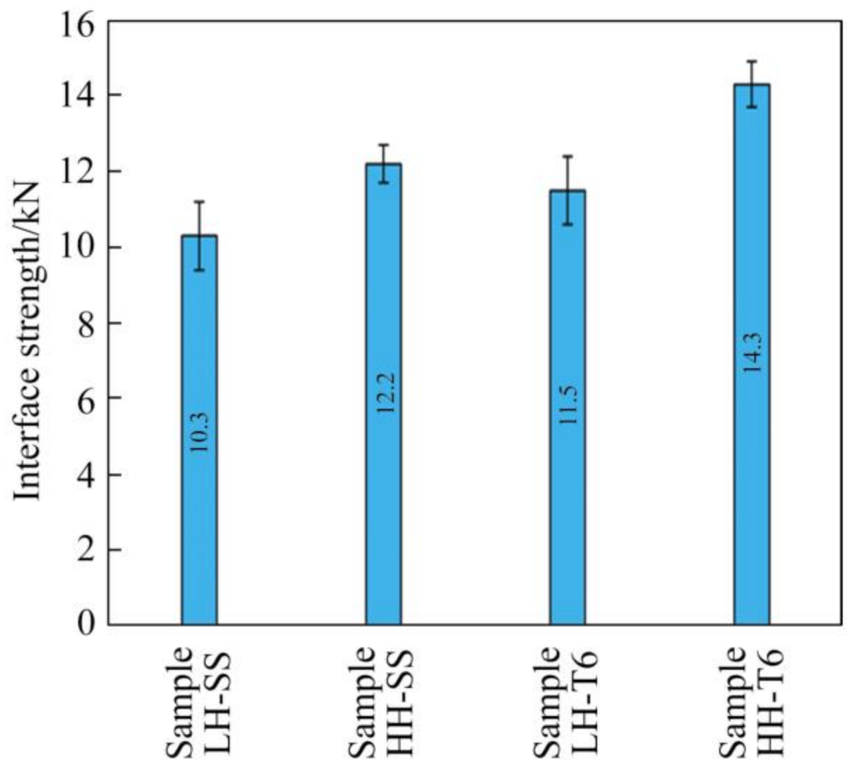

Figure 14 Interface bond strength of different samples

surface and the formation of the coating with a minimum unbonded zone, the bond strength increases. The average bond strength of samples LH-SS, HH-SS, LH-T6, and HH-T6 is (10.3±1.2), (12.2±1.1), (11.5±1.3) and (14.3±2.1) kN, respectively. Meanwhile, coating fabricated with a solid solution-treated rod at a constant heat input reduces the bond strength due to the expansion of the deposited material at a lower area and the formation of larger unbonded zones.

3.4 Wear behavior of coating

According to Figure 15, it can be seen that with increasing normal force, the amount of mass loss of the coating with a solid solution-treated rod changed considerably with constant heat input. This change in the forces in the range of 10 to 30 N is greater than the forces in the range of 30 to 50 N. The wear behavior at forces in the range of 30 to 50 N is similar. Meanwhile, when the normal force increases from 30 to 50 N, the wear rate of the coating fabricated with the artificially aged rod suddenly increases. Figure 16 shows that a similar trend can be seen in the wear diagrams. The wear loss of samples LH-SS, HH-SS, LH-T6, and HH-T6 at load 30 N is (6.7±1.1), (7.6±1.1), (2.7±1.2) and (4.2±1.2) μg/m, respectively. The behavior observed in the coated samples with solid solution-treated and artificially aged rods can be explained by the difference in the dimensions of particles and precipitates.

Since wear is a surface phenomenon and the reinforcements on the surface are under the force's local effect, the size and distribution of the reinforcements on the surface are of particular importance. In the case of the coating created with the solid solution-treated consumable rod, the distance between the reinforcements is more significant than that created with the artificially aged rod. It should also be noted that a similar trend occurs in coatings with increased heat input. During wear, a protective mechanically mixed layer (MML) is formed on the surface by wear chips and materials transferred from the wear surfaces. The closer the average distance of the reinforcements to each other, the more the coating's ability to maintain the MML layer, and as a result, the wear resistance improves. The closer distance between reinforcements also causes the plastic flow of the metal to be controlled. In the case of the coating created with the solid solution-treated rod, on the wear surface, the aluminum matrix is larger than the

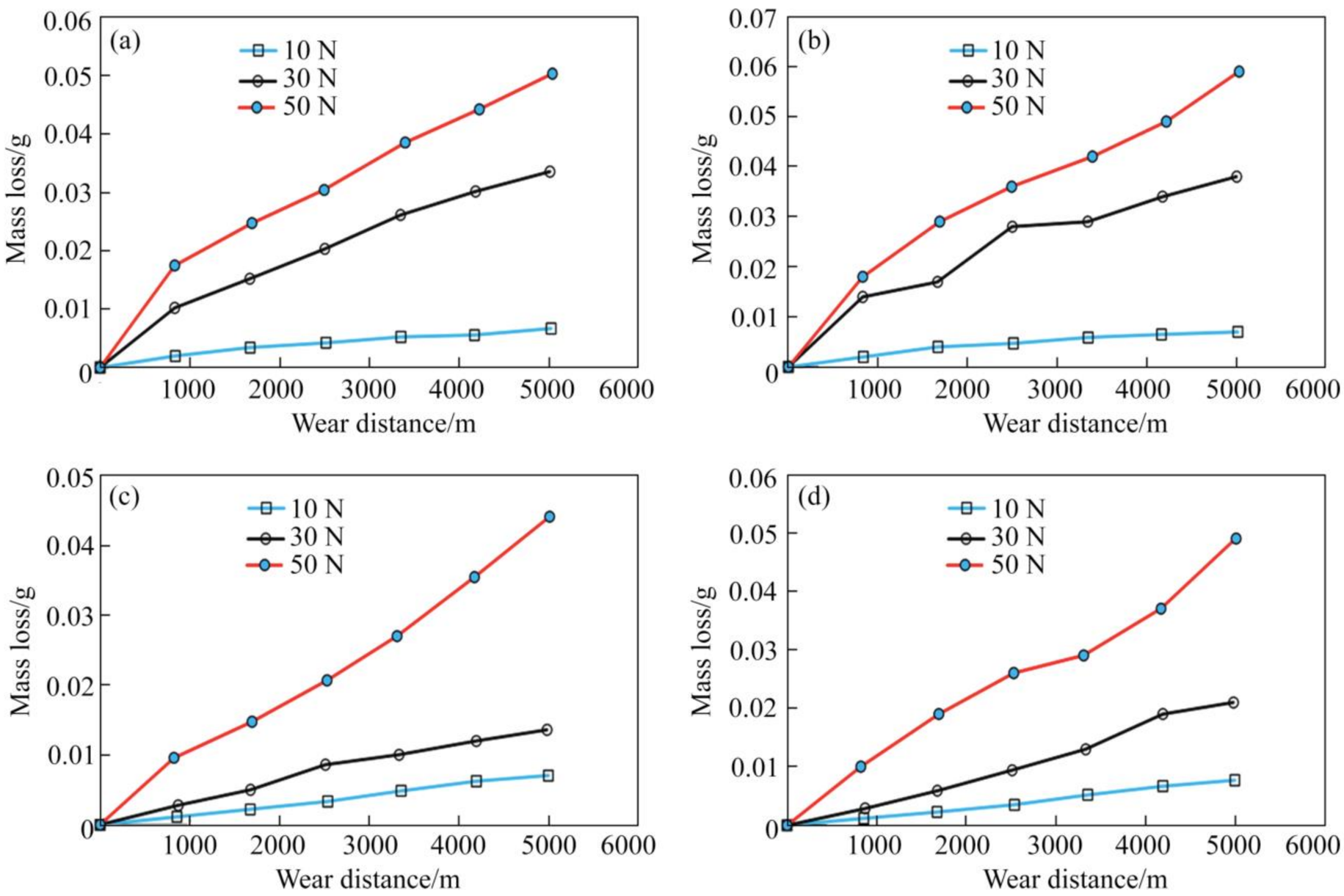

Figure 15 Mass loss versus wear distance: (a) Sample LH-SS; (b) Sample HH-SS; (c) Sample LH-T6; (d) Sample HH-T6

coating created with the artificially aged rod.

For this reason, there is more metal with a low hardness on the surface of the coating created with the solid solution-treated consumable rod compared to the coating created with the artificially aged rod, and this issue causes the coating created with the solid solution-treated rod to be more susceptible to wear. According to Figures 15 and 16, the coating created with the solid solution-treated consumable rod has shown good resistance against low forces, but it has suffered more severe wear when faced with more forces. Also, considering that the reinforcement is present with a more scattered distribution on the surface, it has less resistance to wear. However, due to the more uniform distribution of the reinforcement on the surface, the coating created with the artificially aged rod has good wear resistance up to a load of 26 N. However, at a load of 52 N, its wear resistance has been dramatically reduced. This can be related to increased stress, which is higher than the critical value. In this condition, if the interface between the matrix and the reinforcement is not strong enough, the parts separated from the reinforcement will become wear chips and become a factor increasing the wear. There are two main reasons for improving the wear behavior by reducing the heat input. First of all, due to the reduction of heat input, finer precipitates are created in the aluminum matrix, and as a result, the hardness of the matrix increases. In this way, the resistance of the matrix against the penetration of surfaces and particles will increase, and the amount of wear will decrease. The second reason for the improvement of wear behavior is the increase in the amount of soluble elements in the aluminum matrix. The presence of elements in the form of a solid solution in the aluminum matrix can increase the hardness through the strengthening mechanism of the solid solution. According to Figure 17, it can be seen that under the normal force of 26 N, the coating created with the solid solution-treated rod has suffered severe wear, and the adhesive wear and plastic flow of material at the surface can be seen. In the coating created with the artificially aged rod, transverse cracks and abrasive wear mechanism marks form on the wear surface. Meanwhile, with the increase in heat input in both coatings created with the solid solution-treated rod and the artificially aged rod, the contribution of adhesive wear will increase compared to abrasive wear, and an increase in surface wear will occur.

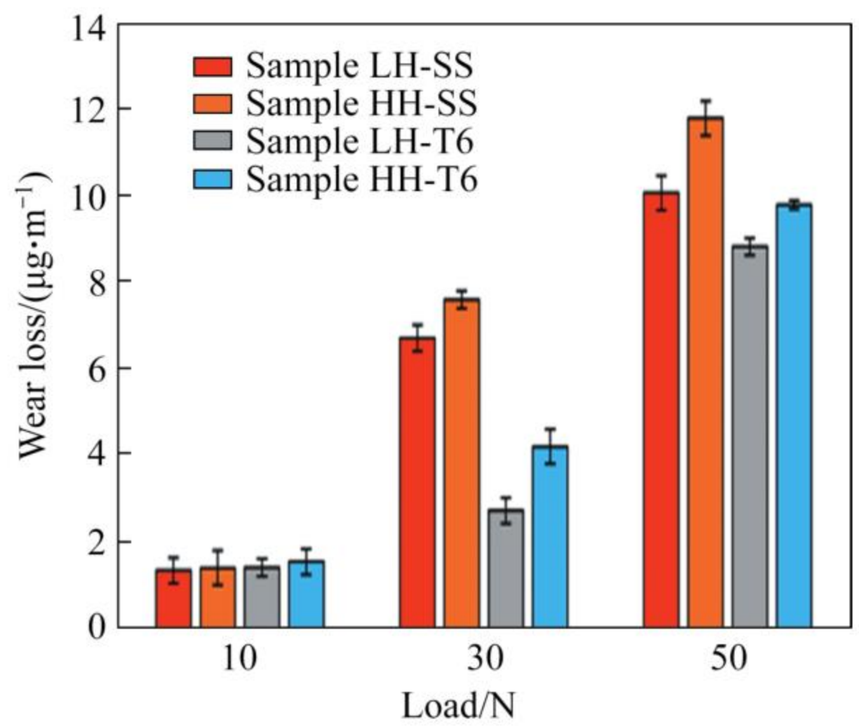

Figure 16 Wear loss of different samples

4 Conclusions

The effects of consumable rod heat treatment and heat input during friction surfacing on the microstructure, mechanical properties, and tribological behavior of hypereutectic Al-Si alloy friction surfaced on commercial pure aluminum were investigated. The main findings are as follows.

1) With the increase in heat input, the coating efficiency increases by 20% and 30% in the solid solution-treated rod and the artificially aged rod, respectively;

2) By increasing heat input, the average grain size in the coating fabricated by solid solution-treated rod and artificially aged rod increases by 10% and 20%, respectively;

3) In constant heat input, the size of the iron-rich and copper-rich particles in the coating created in the solid solution-treated rod is more significant than that of the artificially aged rod;

4) By increasing heat input, the average size of the iron-rich and copper-rich particles in the coating fabricated by a solid solution-treated rod increased from 0.1 to 0.9 μm and 0.2 to 1.3 μm, respectively. Also, by increasing heat input, the average size of the iron-rich and copper-rich particles in the coating fabricated by artificially aged rods increases from 0.1 to 0.9 μm and 0.2 to 1.3 μm, respectively;

5) The average hardness of the coating decreases with the increase in heat input in both the

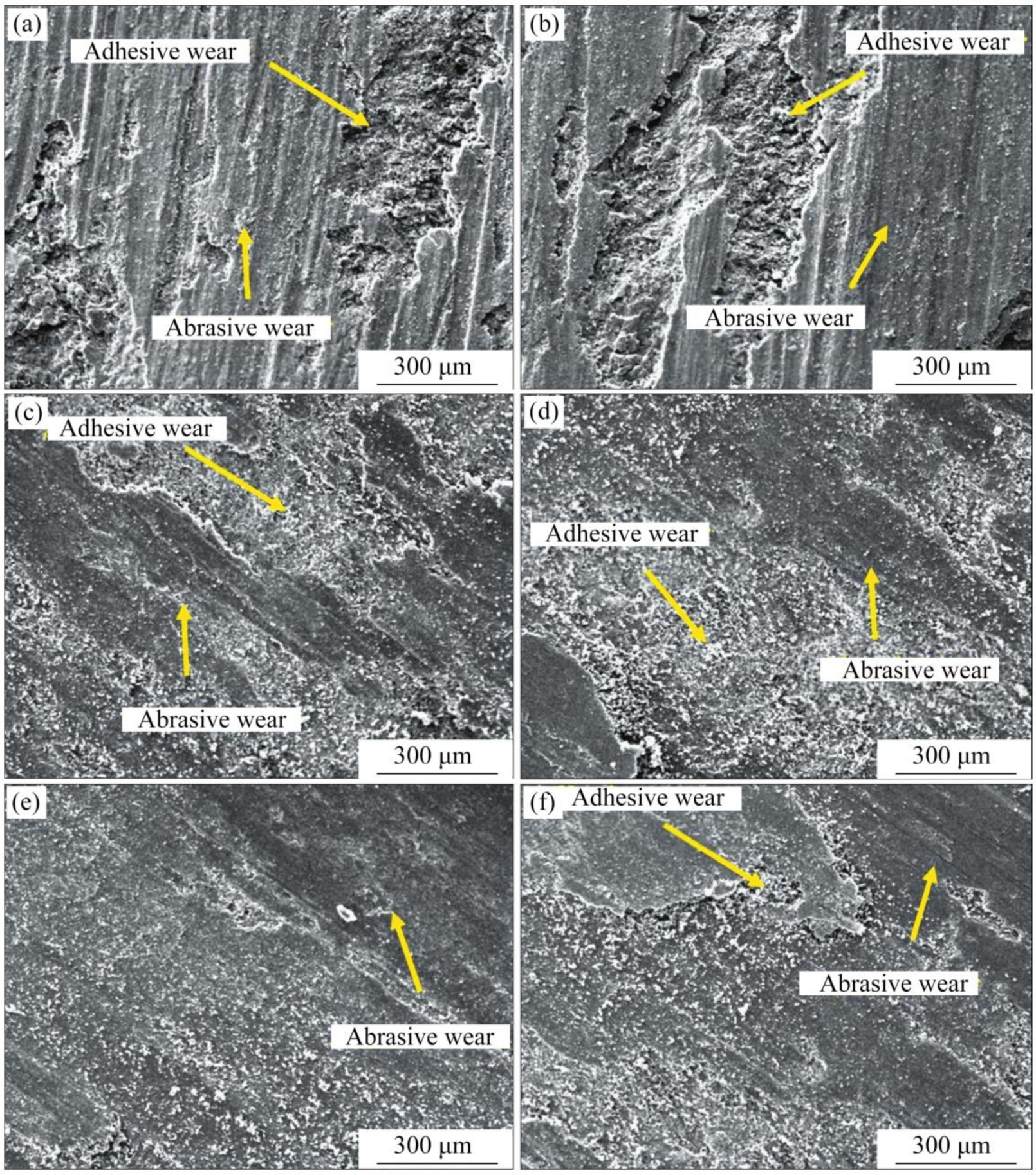

Figure 17 SEM images of worn surface: (a) Solid solution treated consumable rod; (b) Artificially aged consumable rod; (c) Sample LH-SS; (d) Sample HH-SS; (e) Sample LH-T6; (f) Sample HH-T6

coating created with the solid solution-treated and the artificially aged consumable rod. By increasing heat input, the average hardness of the coating fabricated by solid solution-treated rod and artificially aged rod decreases from $HV_{0.1}$ 100 to $HV_{0.1}$ 92 and $HV_{0.1}$ 120 to $HV_{0.1}$ 103, respectively;

6) The average coating/interface bond strength decreases with the decrease in heat input in both the coating created with the solid solution-treated and artificially aged consumable rods. By increasing heat input, the average coating/interface bond strengths of the coating fabricated by solid solution-treated rod and artificially aged rod increase from 10 to 12 kN and 12 to 14 kN, respectively.

7) By decreasing heat input, the wear loss in the coating fabricated by solid solution-treated rod and artificially aged rod decreases by 10% and 20%, respectively, reaching 0.10 and 0.03 μg/m.

Contributors

BARARPOUR Seyedeh Marjan participated in investigation, resources, and writing – original draft. JAMSHIDI AVAL Hamed participated in conceptualization, methodology, writing – review & editing, and supervision. JAMAATI Roohollah participated in conceptualization, methodology, writing – review & editing, and supervision. JAVIDANI Mousa participated in conceptualization,

methodology, writing – review & editing, and supervision.

Conflict of interest

BARARPOUR Seyedeh Marjan, JAMSHIDI AVAL Hamed, JAMAATI Roohollah, and JAVIDANI Mousa declare that they have no conflict of interest.

References

[1] OKOKPUJIE I P, TARTIBU L K, MUSA-BASHEER H O, et al. Effect of coatings on mechanical, corrosion and tribological properties of industrial materials: A comprehensive review [J]. Journal of Bio- and Tribo-Corrosion, 2023, 10(1): 2. DOI: 10.1007/s40735-023-00805-1.

[2] YANG Kun, WANG Jian, YANG Guang-yu, et al. Improved mechanical and wear properties of Ti-35Nb-5Ta-7Zr-xSi alloys fabricated by selective electron beam melting for biomedical application [J]. Journal of Central South University, 2022, 29(12): 3825−3835. DOI: 10.1007/s11771-022-5203-6.

[3] YANG Yi-long, ZHANG Yun, ZHANG Hao-ming, et al. Effect of TiC nanoparticle on friction and wear properties of TiC/AA2219 nanocomposites and its strengthening mechanism [J]. Journal of Central South University, 2022, 29(3): 767−779. DOI: 10.1007/s11771-022-4952-6.

[4] LI Meng-jia, LIAN Juan, CAO Ling-fei, et al. Effect of platform temperature on microstructure and corrosion resistance of selective laser melted Al-Mg-Sc alloy plate [J]. Journal of Central South University, 2022, 29(3): 999−1014. DOI: 10.1007/s11771-022-4959-z.

[5] WANG Qing-hua, WANG Hui-xin. Laser surface functionalization to achieve extreme surface wetting conditions and resultant surface functionalities [J]. Journal of Central South University, 2022, 29(10): 3217 − 3247. DOI: 10.1007/s11771-022-5140-4.

[6] SHI Wen-tian, LI Ji-hang, LIU Yu-de, et al. Experimental study on mechanism of influence of laser energy density on surface quality of Ti-6Al-4V alloy in selective laser melting [J]. Journal of Central South University, 2022, 29(10): 3447−3462. DOI: 10.1007/s11771-022-5135-1.

[7] KHALLAF A H, BHLOL M, DAWOOD O M, et al. Wear resistance, hardness, and microstructure of carbide dispersion strengthened high-entropy alloys [J]. Journal of Central South University, 2022, 29(11): 3529 − 3543. DOI: 10.1007/s11771-022-5181-8.

[8] YUAN Bei, LIAO Dun-ming, JIANG Wen-ming, et al. Effect of friction stir processing on microstructure and friction and wear properties of as-cast SiC_p/ZL101 composites [J]. Journal of Central South University, 2023, 30(10): 3221−3236. DOI: 10.1007/s11771-023-5457-7.

[9] RENNER P, JHA S, CHEN Yan, et al. A review on corrosion and wear of additively manufactured alloys [J]. Journal of Tribology, 2021, 143(5): 050802. DOI: 10.1115/1.4050503.

[10] XIAO Ya, XIONG Ji, GUO Zhi-xing, et al. Microstructures and properties of PVD TiAlN coating deposited on cermets with different Ti(C, N) grain size [J]. Journal of Central South University, 2020, 27(3): 721 − 735. DOI: 10.1007/s11771-020-4326-x.

[11] HANKE S, DOS SANTOS J F. Comparative study of severe plastic deformation at elevated temperatures of two aluminium alloys during friction surfacing [J]. Journal of Materials Processing Technology, 2017, 247: 257−267. DOI: 10.1016/j.jmatprotec.2017.04.021.

[12] ZHU Li-da, XUE Peng-sheng, LAN Qing, et al. Recent research and development status of laser cladding: A review [J]. Optics & Laser Technology, 2021, 138: 106915. DOI: 10.1016/j.optlastec.2021.106915.

[13] FARAJOLLAHI R, JAMSHIDI AVAL H, JAMAATI R, et al. Non-isothermal aging behavior of a friction-surfaced Al-Cu-Mg alloy matrix composite coating reinforced by nickel-aluminide [J]. Journal of Central South University, 2023, 30(11): 3696−3708. DOI: 10.1007/s11771-023-5438-x.

[14] GÜNEN A, GÜROL U, KOÇAK M, et al. A new approach to improve some properties of wire arc additively manufactured stainless steel components: Simultaneous homogenization and boriding [J]. Surface and Coatings Technology, 2023, 460: 129395. DOI: 10.1016/j.surfcoat.2023.129395.

[15] MIRANDA R M, GANDRA J P, VILACA P, et al. Surface modification by solid state processing [M]. Woodhead Publishing, 2014.

[16] EHRICH J, ROOS A, KLUSEMANN B, et al. Influence of Mg content in Al alloys on processing characteristics and dynamically recrystallized microstructure of friction surfacing deposits [J]. Materials Science and Engineering A, 2021, 819: 141407. DOI: 10.1016/j.msea.2021.141407.

[17] PIRHAYATI P, JAMSHIDI AVAL H. Phase-field microstructure simulation during aluminum alloy friction surfacing [J]. Surface and Coatings Technology, 2020, 402: 126496. DOI: 10.1016/j.surfcoat.2020.126496.

[18] GAO H T, KONG C, YU H L. Lightweight metal laminated plates produced via (hot, cold and cryogenic) roll bonding: A review [J]. Transactions of Nonferrous Metals Society of China, 2023, 33(2): 337−356. DOI: 10.1016/S1003-6326(22)66111-9.

[19] KLOPSTOCK H, NEELANDS A R. An improved method of joining or welding metals [P]. UK, No. 572789. [1941-12-20].

[20] AKBARI M, ASADI P, SADOWSKI T. A review on friction stir welding/processing: Numerical modeling [J]. Materials, 2023, 16(17): 5890. DOI: 10.3390/ma16175890.

[21] RATH L, KALLIEN Z, ROOS A, et al. Anisotropy and mechanical properties of dissimilar Al additive manufactured structures generated by multi-layer friction surfacing [J]. The International Journal of Advanced Manufacturing Technology, 2023, 125(5): 2091 − 2102. DOI: 10.1007/s00170-022-10685-3.

[22] ZHOU Li, YU Ming-run, LIU Bai-yang, et al. Microstructure and mechanical properties of Al/steel dissimilar welds fabricated by friction surfacing assisted friction stir lap welding [J]. Journal of Materials Research and Technology, 2020, 9(1): 212−221. DOI: 10.1016/j.jmrt.2019.10.046.

[23] RAHMATI Z, JAMSHIDI AVAL H, NOUROUZI S, et al. Effect of friction surfacing parameters on microstructure and mechanical properties of solid-solutionized AA2024

aluminium alloy cladded on AA1050 [J]. Materials Chemistry and Physics, 2021, 269: 124756. DOI: 10.1016/j.matchemphys.2021.124756.

[24] SEIDI E, MILLER S F, CARLSON B E. Friction surfacing deposition by consumable tools [J]. Journal of Manufacturing Science and Engineering, 2021, 143(12): 120801. DOI: 10.1115/1.4050924.

[25] KALLIEN Z, RATH L, ROOS A, et al. Experimentally established correlation of friction surfacing process temperature and deposit geometry [J]. Surface and Coatings Technology, 2020, 397: 126040. DOI: 10.1016/j.surfcoat.2020.126040.

[26] YU Ming-run, ZHAO Hong-yun, ZHANG Zi-li, et al. Texture evolution and corrosion behavior of the AA6061 coating deposited by friction surfacing [J]. Journal of Materials Processing Technology, 2021, 291: 117005. DOI: 10.1016/j.jmatprotec.2020.117005.

[27] FARAJOLLAHI R, JAMSHIDI AVAL H, JAMAATI R, et al. Effects of pre- and post-friction surfacing heat treatment on microstructure and corrosion behavior of nickel-aluminide reinforced Al-Cu-Mg alloy [J]. Journal of Alloys and Compounds, 2022, 906: 164211. DOI: 10.1016/j.jallcom.2022.164211.

[28] GANDRA J, VIGARINHO P, PEREIRA D, et al. Wear characterization of functionally graded Al – SiC composite coatings produced by Friction Surfacing [J]. Materials & Design, 2013, 52: 373 – 383. DOI: 10.1016/j. matdes. 2013. 05.059.

[29] SHARMA A, SAGAR S, MAHTO R P, et al. Surface modification of Al6061 by graphene impregnation through a powder metallurgy assisted friction surfacing [J]. Surface and Coatings Technology, 2018, 337: 12 – 23. DOI: 10.1016/j.surfcoat.2017.12.059.

[30] ZHAO Jun-wen, WU Shu-sen. Microstructure and mechanical properties of rheo-diecasted A390 alloy [J]. Transactions of Nonferrous Metals Society of China, 2010, 20: s754−s757. DOI: 10.1016/S1003-6326(10)60576-6.

[31] AKBARI M, ASADI P, ZOLGHADR P, et al. Multicriteria optimization of mechanical properties of aluminum composites reinforced with different reinforcing particles type [J]. Journal of Process Mechanical Engineering, 2018, 232(3): 323−337. DOI: 10.1177/095440 8917704994.

[32] PRABHU V V K N. Review of microstructure evolution in hypereutectic Al-Si alloys and its effect on wear properties [J]. Transactions of the Indian Institute of Metals, 2014, 67 (1): 1−18. DOI: 10.1007/s12666-013-0327-x.

[33] AKBARI M, ASADI P, ASIABARAKI H R. Investigation of wear and microstructural properties of a356/TiC composites fabricated by fsp [J]. Surface Review and Letters, 2022, 29(10): 2250130. DOI: 10.1142/s0218625x2250130x.

[34] AKBARI M, ASADI P, ALIHA M R M, et al. Modeling and optimization of process parameters of the piston alloy-based composite produced by fsp using response surface methodology [J]. Surface Review and Letters, 2023, 30(6): 2350041. DOI: 10.1142/S0218625X23500415.

[35] BARARPOUR S M, JAMSHIDI AVAL H, JAMAATI R, et al. Experimental study and thermo-mechanical simulation of friction surfacing treated A390 aluminum alloy [J]. Metals and Materials International, 2024, 30(4): 1072 – 1094. DOI: 10.1007/s12540-023-01561-0.

[36] BARARPOUR S M, JAMSHIDI AVAL H, JAMAATI R, et al. Experimental and numerical investigation of $Al_{16}Si$ alloy friction surfacing on AA1050 aluminum substrate: Effect of axial feeding rate [J]. Surface and Coatings Technology, 2023, 468: 129778. DOI: 10.1016/j.surfcoat.2023.129778.

[37] BARARPOUR S M, JAMSHIDI AVAL H, JAMAATI R, et al. Comparison of finite element and smoothed-particle hydrodynamics models in the simulation of hypereutectic Al-Si alloy friction surfacing: Calibrations from experiments [J]. Archives of Civil and Mechanical Engineering, 2023, 23(4): 224. DOI: 10.1007/s43452-023-00755-y.

[38] SCHÜTTE M R, EHRICH J, LINSLER D, et al. Effects of microstructure modification by friction surfacing on wear behavior of Al alloys with different Si contents [J]. Materials, 2022, 15(5): 1641. DOI: 10.3390/ma15051641.

[39] RAHMATI Z, VAL H J, NOUROUZI S, et al. Effects of pre-heat treatment of the consumable rod on the microstructural and mechanical properties of the friction surfaced Al-Cu-Mg alloy over pure aluminum [J]. Surface and Coatings Technology, 2021, 410: 126954. DOI: 10.1016/j.surfcoat.2021.126954.

[40] GUDURU R K, DARLING K A, KISHORE R, et al. Evaluation of mechanical properties using shear-punch testing [J]. Materials Science and Engineering A, 2005, 395(1, 2): 307−314. DOI: 10.1016/j.msea.2004.12.048.

[41] NIXON R G S, MOHANTY B S, SATHISH R. Friction surfacing of AISI 316 over mild steel: A characteriation study [J]. Defence Technology, 2018, 14(4): 306 – 312. DOI: 10.1016/j.dt.2018.03.003.

[42] GANDRA J, KROHN H, MIRANDA R, et al. Friction surfacing—A review [J]. Journal of Materials Processing Technology, 2014, 214(5): 1062 – 1093. DOI: 10.1016/j.jmatprotec.2013.12.008.

[44] EHRICH J, STARON P, KARKAR A, et al. Precipitation evolution in the heat-affected zone and coating material of AA2024 processed by friction surfacing [J]. Advanced Engineering Materials, 2022, 24(11): 2201019. DOI: 10.1002/adem.202201019.

[45] ALANEME K K, OKOTETE E A. Recrystallization mechanisms and microstructure development in emerging metallic materials: A review [J]. Journal of Science: Advanced Materials and Devices, 2019, 4(1): 19 – 33. DOI: 10.1016/j.jsamd.2018.12.007.

[46] ROLLETT A, ROHRER G S, HUMPHREYS J. Recrystallization and related annealing phenomena [M]. Elsevier, 2017.

[47] BARARPOUR S M, JAMSHIDI AVAL H, JAMAATI R. Modeling and experimental investigation on friction surfacing of aluminum alloys [J]. Journal of Alloys and Compounds, 2019, 805: 57 – 68. DOI: 10.1016/j. jallcom. 2019.07.010.

(Edited by FANG Jing-hua)

中文导读

过共晶Al-Si合金在工业纯铝上的摩擦堆焊：自耗棒热处理和热输入的影响

摘要：本文探讨了自耗棒的预摩擦堆焊热处理和摩擦堆焊过程中的热输入对沉积在工业纯铝基材上的过共晶Al-Si合金的微观结构、力学性能和耐磨性的影响。结果表明，无论在何种自耗棒的热处理条件下，涂层效率都随着热输入的增加而提高，固溶处理棒和人工老化棒的涂层效率分别提高了20%和30%。随着热输入增加，固溶处理棒和人工老化棒制备的涂层中的平均晶粒尺寸分别从0.1和0.2 μm增加到0.9和1.3 μm。在恒定的热输入下，使用固溶处理棒制备涂层的平均硬度和耐磨性低于人工老化棒的。而减少热输入，固溶处理棒和人工老化棒制成的涂层的磨损量分别降低了10%和20%，达到0.1和0.03 μg/m。

关键词：摩擦堆焊；过共晶Al-Si合金；热输入；微观结构；耐磨性